

A theoretical framework for calibrating the depth-dependent optical scattering in layered human skin using spatially-offset measurements

SHUQUAN XIAO,¹ YUNXU SUN,¹ MARTHA VARDAKI,^{2,3} AND WEI LIU^{1,4,*}

¹Optical Imaging Laboratory, Harbin Institute of Technology, Shenzhen, China

²Department of Medical Physics, School of Health Sciences, University of Ioannina, 45110 Ioannina, Greece

³Institute of Chemical Biology, National Hellenic Research Foundation, 48 Vassileos Constantinou Avenue, Athens, 11635, Greece

⁴Quantum Science Center of Guangdong-Hongkong-Macao Greater Bay Area, Shenzhen, China

*Corresponding author: wl157@hit.edu.cn

Received XX Month XXXX; revised XX Month, XXXX; accepted XX Month XXXX; posted XX Month XXXX (Doc. ID XXXXX); published XX Month XXXX

Spatially-offset spectroscopy offers an alternative noninvasive method for enabling deep probing of structures and chemical molecules, which is clinically significant for the characterization of chemical and physical alterations in human skin. However, a more precise depth-resolved quantification using the spatially-offset measurements still remains as a challenge due to the mixed inhomogeneous scattering. Herein, we report a Monte-Carlo-based quantification modelling platform combined with a novel scattering spectrum decomposition method to explore the depth-dependent optical scattering contributions in human skin. In the simplified modelling, human skin was empirically set to be composed of three layers and each layer possessed different photon weights for the spatially-offset scattering intensity measurements. The modelling results of photon transportation in-and-out of the layered skin substantially discovered that the layer-dependent scattering contribution was compositely encoded into the spatially-offset measurements and varied with the illumination incidence angle. For calibrating the layer-dependent scattering contribution, a modified nonlinear independent component processing algorithm was applied to the spatially-offset measurements by decomposing the photon weights of each layer. The calibration results figured out the major scattering contribution of each layer along the offset axis under different incidence angles, which were consistent with previously experimental observations. The proposed theoretical framework establishes a feasible approach for spatially-offset optical spectroscopies enabling non-invasive quantitative A-line characterization of the concentrations of skin components. © 2024 Optica Publishing Group

As living tissues comprised of inhomogeneous molecular components randomly disordering the light propagation inside [1], optical scattering is the key challenge to translate the state-of-the-art optical imaging and measurement technologies to a wider field of clinical impact. Though optical clearing technologies have been successfully applied to various biological tissues to reduce optical scattering and enable deep probing of large volumes [2, 3], one important complication caused by the invasive clearing is the loss of tissue functions. In the meantime, a few non-invasive technologies have been proposed to guide the forward propagation of the photons in thick scattering tissues, including ultrasound encoding [4-6] and wavefront shaping[7-9], which were not targeted at addressing the issue of unpredictable photon backscattering in probing deep tissues.

The recently developed Spatially-Offset Raman Spectroscopy (SORS) is a non-invasive alternative approach for probing deep tissues [10, 11], which enables depth-sensitive scattering spectrum

analysis using spatially-offset measurements. Though SORS achieved success in characterization of thick tissues [10, 12], poor depth resolution was suffered due to diffuse scattering, even utilizing focused illumination and detection [13]. Another challenge in SORS is to extract the pure spectrum contributed by the different tissue layers, as the photons scattered from different layers were mixed in each offset. In order to improve the sectioning performance of the spatially-offset measurements, it is required to calibrate the scattering contribution of each layer along the transverse offsets. To date, there are few reports on calibrating the specific depth contribution using spatially-offset measurements, except for applying both scattering and absorption matrices which, however, is not applicable to all *in vivo* measurements especially where transmission mode is required [12, 14, 15].

Herein, we are presenting a Monte-Carlo-based proof-of-concept study of calibrating the depth-dependent scattering contribution

using spatially-offset measurements. For simplicity, this feasibility study is focused on healthy human skin model for which the geometric and optics properties have been thoroughly investigated [16, 17]. Without loss of generality, the human skin model was set to be composed of three layers, i.e., epidermis, papillary dermis, and reticular dermis, as shown in **Fig. 1**. It needs to be stated that the epidermis was simplified to be one layer instead of four strata (including the stratum corneum) and the subcutaneous layer was also assumed to be the penetration boundary (~ 2 mm) if applying a small (diameter: 1 mm) illumination spot. The other skin modeling parameters, including thickness, scattering coefficient, absorption coefficient, and refractive index are presented in **Supplemental Tab. S1**. It is worth mentioning that the parameter values of each skin layer can be varied on the basis of race, gender, age, and body site [18, 19], thus the calibration can be highly application-driven.

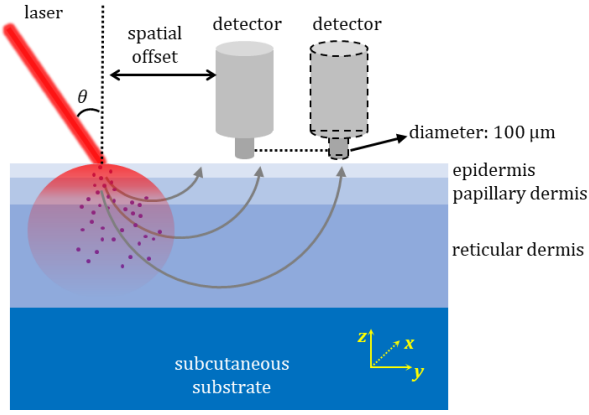


Fig. 1. A conventional fiber-coupled spatially-offset configuration for layered human skin tissues. θ indicates illumination incidence angle. The offset indicates the detector displacement to the incident point.

A modified variance reduction Monte-Carlo (VRMC) algorithm [20-23] was then applied for high-speed tracking of the photon transportation in the layered skin model. The numerical simulation was confined to the conventional spatially-offset measurement configuration (see **Fig. 1**) and utilized photon weight for quantifying the left intensity of one photon after experiencing a random scattering. The initial photon weight of an arbitrary photon at the incident surface is given by

$$W = 1 - \frac{(n_{air} - n_{epi})^2}{(n_{air} + n_{epi})^2}, \quad (1)$$

where n_{air} and n_{epi} indicate the refraction index of air and epidermis, respectively. Inside the skin tissue, the photon weight of the specific photon is concomitantly decreased per scattering event by multiplying the following attenuation factor

$$W_s = \frac{\mu_s}{\mu_t}, \quad (2)$$

where μ_s is the scattering coefficient and μ_t is the total attenuation coefficient. It should be pointed out that each skin layer possesses different attenuation factors as their absorption and scattering coefficient values are different (see **Supplemental Tab. S1**). A minimum threshold of the photon weight has been preset to determine the lifetime of a photon, below which the photon was considered to be totally absorbed or out of boundary. The flow chart of the VRMC simulation of one-photon transportation and photon

weight update is shown in **Fig. 2**. Following a random scattering pathlength, the photon weight was iteratively updated by multiplying W_s , and a Russian Roulette method was applied in VRMC for determining whether the photon weight should be zeroed after reaching the preset photon weight threshold.

According to the VRMC simulation procedure, the transportation path of the incident photons in layered human skin can be figured out (see **Supplemental Fig. S1**). More importantly, the spatial distribution of the photon weight of the out photons (out of tissue) can be tracked with layer labels, and the total weight of each layer was superimposed by the labelled weights. For statistical significance, 10^6 incident photons in total were employed to investigate the spatially-offset scattering distribution with different incidence angles. When the incidence angle was changed from 0 degree (normal incidence) to 60 degrees (oblique incidence), the center of scattering photons had a transverse shift to the incident point, as shown in **Figs. 3A-B**. This observation can be further confirmed by quantifying the photon weight of each layer along the transverse direction with a confined-size fiber detector (diameter: 100 μm), as shown in **Figs. 3C-D**. It is also found that the out photons experience transverse shift and the deeper photons have the larger shift while increasing the incidence angle, as shown in **Fig. 3E**. The VRMC simulation results of the photon transportation in layered human skin verify that the depth-dependent scattering is encoded into the spatially-offset intensity transient and oblique incidence can improve the depth-resolve performance.

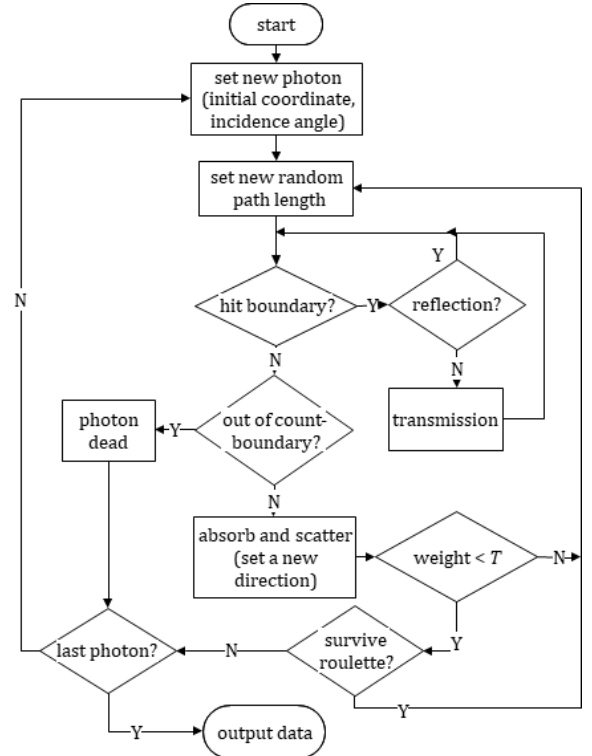


Fig. 2. Simulation flow chart of one-photon transportation and photon weight update using Russian-Roulette modified VRMC algorithm.

It should be pointed out that total photon weight (TPW) distributions of epidermis are equivalent to the experimentally spatially-offset intensity measurements as all out photons went through the first layer. Taking into account of the fact that each skin layer is an independent scattering source, the TPW of epidermis can

be considered as the mixture of these sources. A calibration method is then required to resolve the individual scattering contribution of each layer from the spatially-offset intensity measurements.

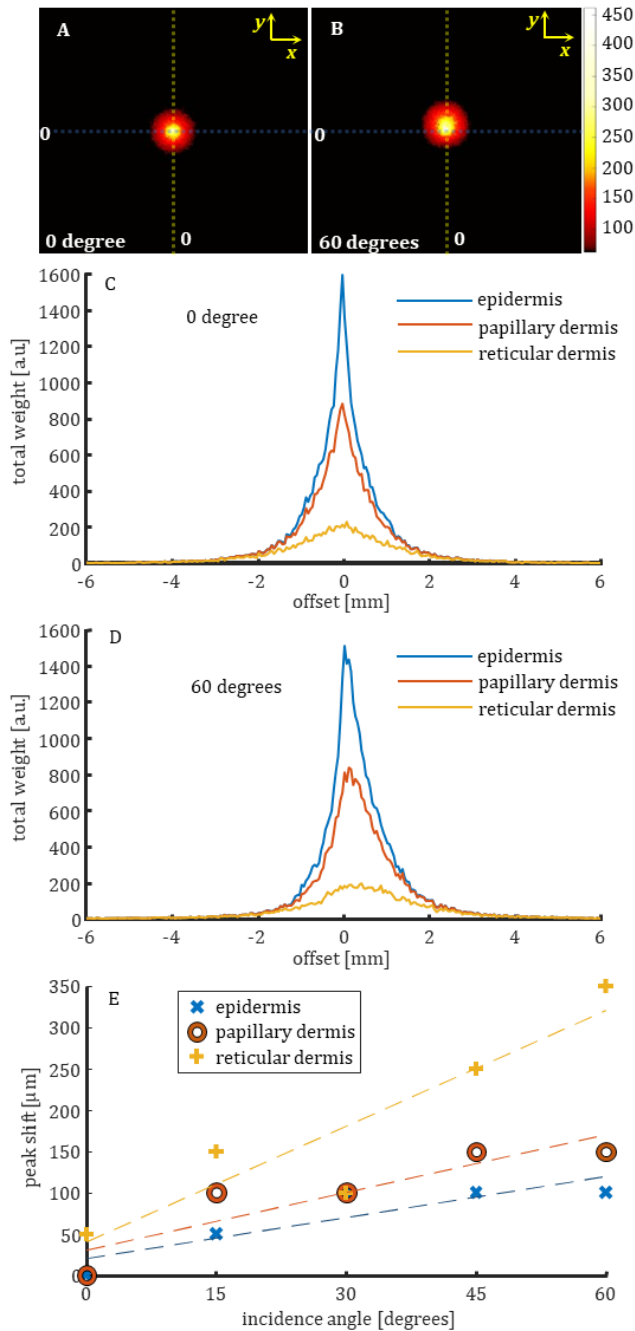


Fig. 3. VRMC-based numerical results of spatially-offset scattering photon weights with different incidence angles. A-B, top views (0 and 60 degrees), color bar: photon weight number; C-D, the fiber (diameter: 100 μm) measurement profile along the dashed yellow lines in A-B; E, TPW peak-shift of different layers with increasing incidence angles.

Independent component analysis (ICA)-based blind source separation [24] was typically applied to recover the independent source signals, however, ICA cannot deal with positive signals [25-27], such as the photon weights. Herein, a nonlinear independent component processing (NICP) algorithm is proposed to quantify the scattering contribution proportion of each layer per offset using the

TPW of epidermis. The verification of the NICP algorithm using a series of test signals can be found in **Supplement 1**. In NICP, the mixed signal (TPW of epidermis) was first processed by ICA for predicting the unmixed prototype of the individual photon weight of each layer (see **Supplemental Fig. S2B**), and then nonlinear programming (see **Supplemental Eqs. S1-S4**) was applied to further polish the spatially-offset scattering contribution proportion (SSCP) waveform of each layer utilizing the positive-value constraint.

NICP was performed several times to average the output SSCP waveforms. Because the TPW obtained in a large offset (see **Fig. 3**) was in low SNR [28] and thus could be ignored, the SSCP waveforms were only displayed within 3-mm offset, as shown in **Figs. 4A-C**. The SSCP waveforms of different incidence angles showed the similar observations that 1) the scattering dominate area of the superficial layer (epidermis) seems to be independent of the incident angle, whose offset basically falls in the range of [0, 0.4] mm, and 2) the scattering dominant area range of the deeper layers was expanded with the increase of the incidence angle from 0 to 60 degrees, and it was expanded from [0.4, 1.2] mm to [0.4, 1.7] mm for the papillary dermis layer and from [2.4, 3] mm to [1.9, 3] mm for the reticular dermis layer. The expansion of the dominant area would result in a benefit for more precise quantifications of depth-dependent scattering but, on the flip side, it might also cause the degradation of depth-resolve resolution. These depth-dependent scattering observations in the spatially-offset configuration are consistent with previous experiment founding (including our previous work) [13, 15], which verify the effectiveness of the utility of photon weights quantifying the scattering contribution proportion.

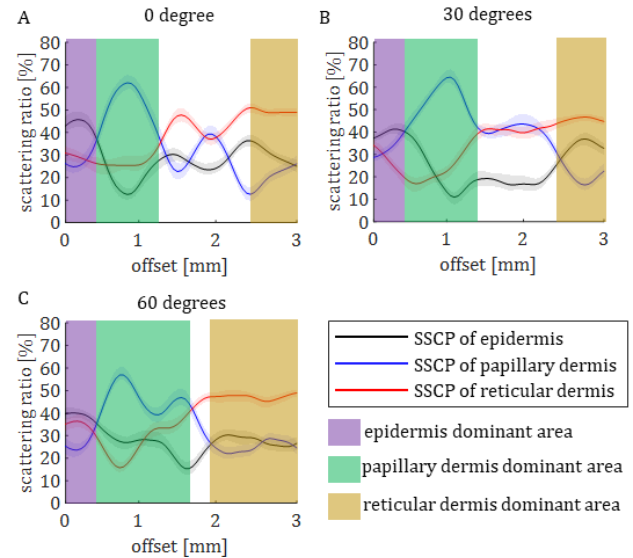


Fig. 4. The numerical-calibrated spatially-offset scattering contribution proportion (SSCP) waveforms of different layers. A-C, the SSCP waveform changes with different incidence angles (0 to 60 degrees).

It is also interesting to discover the scattering dominate area of deep layers has the opposite expansion direction if continuously increasing the oblique incidence angle, as shown in **Fig. 5**. The apparent center of papillary dermis dominant area (PDDA) showed a linear trend (R^2 : 0.68) of being away from the incidence point, while the apparent starting point of reticular dermis dominant area (RDDA) showed a linear trend (R^2 : 0.97) of being close to the incidence point. This phenomenon can be elaborated by the much

larger shift magnitude of the quantitative TPW peaks of reticular dermis compared to papillary dermis (see Fig. 3E).

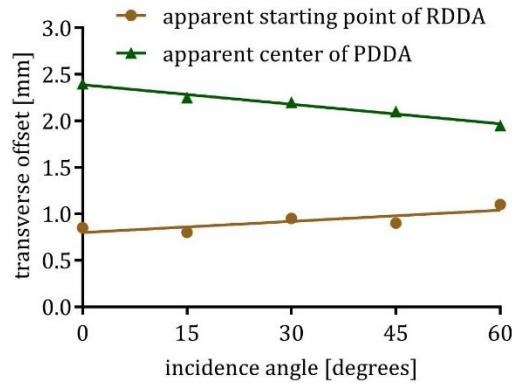


Fig. 5. The spatial offset of the scattering dominate area of deep layers under oblique illumination with different angles. PDDA: papillary dermis dominant area; RDDA: reticular dermis dominant area.

The numerical-calibrated spatial SSCP matrices can be applied for enabling quantitative A-line skin component concentration measurements using the spatially-offset optical spectroscopy instrumentations, since they provide precise photon compensations. Assuming that X is the unknown layer-dependent molecular concentration distribution, P is the SSCP matrices composed of each skin layer, and S is the lateral spatially-offset scattering intensity measurements, then they satisfy the following relationship as

$$S = nPX, \quad (3)$$

where n is the molecular photon conversion efficiency per unit concentration applicable for fluorescence emission or Raman scattering and can be considered as a constant for a specific component. Since the photon weights of each skin layer is independent, the invertible matrix P^{-1} must exist. Hence, the layer-dependent molecular concentration can be calculated by

$$X = (P^{-1}S)/n. \quad (4)$$

The axial resolution of the above quantitative A-line component concentration would be limited as only three depths (i.e., three layers) are provided in the SSCP matrices, which can be further improved by increasing the numbers of simulation photons and skin layers. Another limitation of the utility of the numerical-calibrated SSCP matrices is the ordinary generalization, as the structures and optical parameters of human skin can be varied with gender, race and age.

In conclusion, we have analyzed the photon transportation in layered human skin and quantified the photon weights of each layer using the variance reduction Monte-Carlo (VRMC) method. The numerical VRMC simulation results verified that the layer-dependent scattering was encoded into the spatially-offset intensity transients and could be better resolved with oblique illumination, which were consistent with previous experiment demonstrations. A nonlinear independent component processing algorithm was developed to calibrate the spatially-offset scattering contribution proportion (SSCP) of each skin layer. The numerical-calibrated SSCP matrices can be further applied for achieving A-line spectroscopic measurements of human skin. Future experiment studies will be carried out to maximize the clinical impacts of the proposed theoretical framework.

Funding. National Natural Science Foundation of China (62205089); Basic and Applied Basic Research Foundation of Guangdong Province (2021A1515110030); Guangdong Provincial Quantum Science Strategic Initiative (GDZX2304006); Science, Technology and Innovation Commission

of Shenzhen Municipality (GXWD20231130143453003, SGDXX20220530111403022).

Disclosures. The authors declare no conflicts of interest.

Data availability. Data underlying the results presented in this paper may be obtained from the authors upon reasonable request.

Supplemental document. See Supplement 1 for supporting content.

References

1. J. C. Stover, *Optical scattering: Measurement and analysis* (2012).
2. I. Costantini, R. Cicchi, L. Silvestri, F. Vanzi, and F. S. Pavone, *Biomed. Opt. Express* **10**, 5251-5267 (2019).
3. T. Tian, Z. Yang, and X. Li, **238**, 489-507 (2021).
4. H. Kim, S. Youn, J. Kim, S. Park, M. Lee, J. Y. Hwang, and J. H. Chang, *Nature Photonics* **16**, 762-768 (2022).
5. J. Luo, Y. Liu, D. Wu, X. Xu, L. Shao, Y. Feng, J. Pan, J. Zhao, Y. Shen, and Z. Li, **8**, eadd9158 (2022).
6. J. W. Tay, P. Lai, Y. Suzuki, and L. V. Wang, *Scientific Reports* **4**, 3918 (2014).
7. J. Cao, Q. Yang, Y. Miao, Y. Li, S. Qiu, Z. Zhu, P. Wang, and Z. Chen, *Light: Science & Applications* **11**, 108 (2022).
8. Z. Yu, H. Li, T. Zhong, J.-H. Park, S. Cheng, C. M. Woo, Q. Zhao, J. Yao, Y. Zhou, X. Huang, W. Pang, H. Yoon, Y. Shen, H. Liu, Y. Zheng, Y. Park, L. V. Wang, and P. Lai, *The Innovation* **3**, 100292 (2022).
9. Z. Cheng, C. Li, A. Khadria, Y. Zhang, and L. V. Wang, *Nature Photonics* **17**, 299-305 (2023).
10. F. Nicolson, M. F. Kircher, N. Stone, and P. Matousek, *Chemical Society Reviews* **50**, 556-568 (2021).
11. P. Matousek, *TrAC Trends in Analytical Chemistry* **103**, 209-214 (2018).
12. S. Mosca, C. Conti, N. Stone, and P. Matousek, *Nature Reviews Methods Primers* **1** (2021).
13. W. Liu, Y. H. Ong, X. Yu, J. Ju, C. Perlaki, L. Liu, and Q. Liu, *Optics Express* **24**, 28312-28325 (2016).
14. S. Mosca, P. Dey, T. A. Tabish, F. Palombo, N. Stone, and P. Matousek, *Anal Chem* **91**, 8994-9000 (2019).
15. S. Mosca, P. Dey, M. Salimi, B. Gardner, F. Palombo, N. Stone, and P. Matousek, *Anal Chem* **93**, 6755-6762 (2021).
16. E. Salomatina, B. Jiang, J. Novak, and A. N. Yaroslavsky, *J Biomed Opt* (2006).
17. I. V. Meglinski, and S. J. Matcher, *Physiological Measurement* **23**, 741 (2002).
18. X. Yang, Y. Cui, J. Yue, H. He, C. Yu, P. Liu, J. Liu, X. Ren, and Y. Meng, *PLoS ONE* **12** (2017).
19. P. Oltulu, B. Ince, N. Kökbudak, S. Findik, and F. Kiliç, *Türk Plastik, Rekonstruktif ve Estetik Cerrahi Dergisi* **26**, 56-61 (2018).
20. L. Wang, S. L. Jacques, and L. Zheng, *Computer Methods and Programs in Biomedicine* **47**, 131-146 (1995).
21. S. L. Jacques, *Modeling tissue optics using monte carlo modeling: A tutorial* (SPIE, 2008).
22. C. Zhu, and Q. Liu, *J Biomed Opt* **18**, 50902 (2013).
23. A. A. Leino, A. Pulkkinen, and T. Tarvainen, *OSA Continuum* **2** (2019).
24. M. Pal, R. Roy, J. Basu, and M. S. Bepari, "Blind source separation: A review and analysis," in *2013 International Conference Oriental COCOSA held jointly with 2013 Conference on Asian Spoken Language Research and Evaluation (O-COCOSA/CASLRE)*(2013), pp. 1-5.
25. W. Naanaa, and J.-M. Nuzillard, *Signal Processing* **85**, 1711-1722 (2005).
26. A. Hyvärinen, and E. Oja, *Neural Networks* **13**, 411-430 (2000).
27. Y. Sun, C. Ridge, F. del Rio, A. J. Shaka, and J. Xin, *Signal Processing* **91**, 1838-1851 (2011).
28. M. Z. Vardaki, K. Seretis, G. Gaitanis, I. D. Bassukas, and N. Kourkoumelis, **11**, 9498 (2021).

Complete information of References

1. Stover, J. C., *Optical Scattering: Measurement and Analysis*. Third ed.; SPIE, 2012; Vol. PM224.
2. Costantini, I.; Cicchi, R.; Silvestri, L.; Vanzi, F.; Pavone, F. S., In-vivo and ex-vivo optical clearing methods for biological tissues: review. *Biomed. Opt. Express* **2019**, *10* (10), 5251-5267.
3. Tian, T.; Yang, Z.; Li, X., Tissue clearing technique: Recent progress and biomedical applications. **2021**, *238* (2), 489-507.
4. Kim, H.; Youn, S.; Kim, J.; Park, S.; Lee, M.; Hwang, J. Y.; Chang, J. H., Deep laser microscopy using optical clearing by ultrasound-induced gas bubbles. *Nature Photonics* **2022**, *16* (11), 762-768.
5. Luo, J.; Liu, Y.; Wu, D.; Xu, X.; Shao, L.; Feng, Y.; Pan, J.; Zhao, J.; Shen, Y.; Li, Z., High-speed single-exposure time-reversed ultrasonically encoded optical focusing against dynamic scattering. **2022**, *8* (50), eadd9158.
6. Tay, J. W.; Lai, P.; Suzuki, Y.; Wang, L. V., Ultrasonically encoded wavefront shaping for focusing into random media. *Scientific Reports* **2014**, *4* (1), 3918.
7. Cao, J.; Yang, Q.; Miao, Y.; Li, Y.; Qiu, S.; Zhu, Z.; Wang, P.; Chen, Z., Enhance the delivery of light energy ultra-deep into turbid medium by controlling multiple scattering photons to travel in open channels. *Light: Science & Applications* **2022**, *11* (1), 108.
8. Yu, Z.; Li, H.; Zhong, T.; Park, J.-H.; Cheng, S.; Woo, C. M.; Zhao, Q.; Yao, J.; Zhou, Y.; Huang, X.; Pang, W.; Yoon, H.; Shen, Y.; Liu, H.; Zheng, Y.; Park, Y.; Wang, L. V.; Lai, P., Wavefront shaping: A versatile tool to conquer multiple scattering in multidisciplinary fields. *The Innovation* **2022**, *3* (5), 100292.
9. Cheng, Z.; Li, C.; Khadria, A.; Zhang, Y.; Wang, L. V., High-gain and high-speed wavefront shaping through scattering media. *Nature Photonics* **2023**, *17* (4), 299-305.
10. Nicolson, F.; Kircher, M. F.; Stone, N.; Matousek, P., Spatially offset Raman spectroscopy for biomedical applications. *Chemical Society Reviews* **2021**, *50* (1), 556-568.
11. Matousek, P., Spatially offset Raman spectroscopy for non-invasive analysis of turbid samples. *TrAC Trends in Analytical Chemistry* **2018**, *103*, 209-214.
12. Mosca, S.; Conti, C.; Stone, N.; Matousek, P., Spatially offset Raman spectroscopy. *Nature Reviews Methods Primers* **2021**, *1* (1).
13. Liu, W.; Ong, Y. H.; Yu, X.; Ju, J.; Perlaki, C.; Liu, L.; Liu, Q., Snapshot depth sensitive Raman spectroscopy in layered tissues. *Optics Express* **2016**, *24*, 28312-28325.
14. Mosca, S.; Dey, P.; Tabish, T. A.; Palombo, F.; Stone, N.; Matousek, P., Spatially Offset and Transmission Raman Spectroscopy for Determination of Depth of Inclusion in Turbid Matrix. *Anal Chem* **2019**, *91* (14), 8994-9000.
15. Mosca, S.; Dey, P.; Salimi, M.; Gardner, B.; Palombo, F.; Stone, N.; Matousek, P., Spatially Offset Raman Spectroscopy-How Deep? *Anal Chem* **2021**, *93* (17), 6755-6762.
16. Salomatina E, J. B., Novak J, Yaroslavsky AN, Optical properties of normal and cancerous human skin in the visible and near-infrared spectral range. *J Biomed Opt* **2006**.
17. Igor, V. M.; Stephen, J. M., Quantitative assessment of skin layers absorption and skin reflectance spectra simulation in the visible and near-infrared spectral regions. *Physiological Measurement* **2002**, *23* (4), 741.
18. Yang, X.; Cui, Y.; Yue, J.; He, H.; Yu, C.; Liu, P.; Liu, J.; Ren, X.; Meng, Y., The histological characteristics, age-related thickness change of skin, and expression of the HSPs in the skin during hair cycle in yak (*Bos grunniens*). *PLoS ONE* **2017**, *12*.
19. Oltulu, P.; Ince, B.; Kökbudak, N.; Findik, S.; Kılıç, F., Measurement of epidermis, dermis, and total skin thicknesses from six different body regions with a new ethical histometric technique. *Türk Plastik, Rekonstruktif ve Estetik Cerrahi Dergisi* **2018**, *26*, 56-61.
20. Wang, L.; Jacques, S. L.; Zheng, L., MCML—Monte Carlo modeling of light transport in multi-layered tissues. *Computer Methods and Programs in Biomedicine* **1995**, *47* (2), 131-146.
21. Jacques, S. L., *Modeling tissue optics using Monte Carlo modeling: a tutorial*. SPIE: 2008; Vol. 6854.
22. Zhu, C.; Liu, Q., Review of Monte Carlo modeling of light transport in tissues. *J Biomed Opt* **2013**, *18* (5), 50902.
23. Leino, A. A.; Pulkkinen, A.; Tarvainen, T., ValoMC: a Monte Carlo software and MATLAB toolbox for simulating light transport in biological tissue. *OSA Continuum* **2019**, *2* (3).
24. Pal, M.; Roy, R.; Basu, J.; Bepari, M. S. In *Blind source separation: A review and analysis*, 2013 International Conference Oriental COCODA held jointly with 2013 Conference on Asian Spoken Language Research and Evaluation (O-COCOSDA/CASLRE), 25-27 Nov. 2013; 2013; pp 1-5.
25. Naanaa, W.; Nuzillard, J.-M., Blind source separation of positive and partially correlated data. *Signal Processing* **2005**, *85* (9), 1711-1722.
26. Hyvärinen, A.; Oja, E., Independent component analysis: algorithms and applications. *Neural Networks* **2000**, *13* (4), 411-430.
27. Sun, Y.; Ridge, C.; del Rio, F.; Shaka, A. J.; Xin, J., Postprocessing and sparse blind source separation of positive and partially overlapped data. *Signal Processing* **2011**, *91* (8), 1838-1851.
28. Vardaki, M. Z.; Seretis, K.; Gaitanis, G.; Bassukas, I. D.; Kourkoulis, N., Assessment of Skin Deep Layer Biochemical Profile Using Spatially Offset Raman Spectroscopy. **2021**, *11* (20), 9498.